Proceedings of the 21st ICSMGE, Vienna, Austria, 14 – 19 June 2026. Pistrol, Adam & Schweiger (eds.)
Published by: ÖGG, Austrian Society for Geomechanics, Salzburg, Austria, ISBN 978-3-9503898-4-5
https://doi.org/10.53243/ICSMGE2026-1075

Investigating Crushable Sand Behavior Using X-Ray Imaging

Mohammad Amin Sayyah
Geotechnics Laboratory, Ghent University, Technologiepark 68, 9052 Zwijnaarde, Belgium,
Mohammadamin.Sayyah@ugent.be

Mahya Roustaei
Geotechnics Laboratory, Ghent University, Technologiepark 68, 9052 Zwijnaarde, Belgium
Department of Earth and Atmospheric Sciences, University of Alberta, Edmonton, Canada

Laurenz Schröer, Chandra Widyananda Winardhi
PProGRess-UGCT, Department of Geology, Ghent University, Ghent, Belgium

Arash A. Lavasan
Computational Soil Mechanics and Foundation Engineering, Engineering Department, Faculty of Science, Technology and Medicine, University of Luxembourg, Luxembourg City, Luxembourg

Veerle Cnudde
PProGRess-UGCT, Department of Geology, Ghent University, Ghent, Belgium
Environmental Hydrogeology, Department of Earth Sciences, Utrecht University, Utrecht, the Netherlands

ABSTRACT: Crushable sands, such as calcareous and glauconite sands, are common in geotechnical applications and pose significant challenges due to their tendency to deform and break under loading. In regions like Belgium and the Netherlands, these soils can lead to excessive settlement, strength reduction, unpredictable behavior, drainage issues, compaction difficulties, poor load distribution, and material degradation—ultimately causing structural instability and increased project costs. Understanding the behavior of crushable sands under varying loading conditions is therefore critical in geotechnical engineering. Traditional experimental methods provide limited insight into the internal mechanisms of particle deformation and breakage. To overcome this, we employed X-ray computed tomography (XCT), which offers high-resolution, three-dimensional imaging of internal structures. Using the Deben CT5000, a specialized device for compressive testing within an XCT system, we captured detailed 3D images of sand particles under controlled loading conditions. These images enabled a comprehensive analysis of particle-scale interactions and breakage patterns. Our comparative investigation of calcareous and glauconite sands provided new insights into their distinct deformation and breakage mechanisms. The findings contribute to improved understanding and modeling of crushable sand behavior, with implications that extend beyond geotechnical engineering to applications such as wind turbine foundations, where similar challenges exist.

KEYWORDS: Crushable sands; X-ray computed tomography (XCT); Particle breakage; Calcareous sand; Glauconitic sand.

1 INTRODUCTION

Crushable sands, particularly those composed of weak minerals such as calcium carbonate (in calcareous sands) and glauconite (in glauconitic sands), play a vital role in numerous geotechnical and offshore applications. These sands are widespread in coastal and marine environments including the North Sea, Persian Gulf, and tropical reef regions, where they serve as the foundation for critical infrastructure such as wind turbines, pipelines, and offshore platforms (Heiken, 1974; Folk, 1980; Scoffin, 1987; Zimbelman, 1996; Le Pera and Morrone, 2020; Wu et al., 2021; Belousov et al., 2022; Peng et al., 2024). However, their engineering behavior is significantly different from that of more durable quartz sands. Due to their low hardness, angular morphology, and high initial porosity, these sands are prone to extensive particle breakage under mechanical loading, which in turn affects their compressibility, strength, dilatancy, permeability, and overall structural stability (Hardin, 1985; Nakata et al., 2001; Coop et al., 2004; Valdes and Koprulu, 2007; Wu et al., 2021).

The phenomenon of particle breakage in crushable soils has been studied extensively since the mid-20th century. Seminal research by Terzaghi and Peck (1948), De Souza (JM, 1958), and Marsal (1967) laid the groundwork for understanding the influence of high stress on grain crushing. Subsequent studies have focused on how breakage evolves under different loading paths and stress conditions, and how it affects soil behavior at both micro and macro scales (Lee and Farhoomand, 1967; Seed and Lee, 1967; Vesić and Clough, 1968; Hardin, 1985; Coop and Atkinson, 1993; Hagerty et al., 1993; McDowell, Bolton and Robertson, 1996; Nakata et al., 2001; Coop et al., 2004; Jia et al., 2019). To quantify this behavior, various indices such as Hardin's Relative Breakage (Br), Marsal's Breakage Factor (Bg), and Indraratna's Breakage Index (BI) have been developed based on changes in particle size distribution (Lee and Farhoomand, 1967; Marsal, 1967; Hardin, 1985; Indraratna, Wijewardena and Balasubramaniam, 1993).

Despite the wide use of triaxial, oedometer, ring shear, and single-grain tests to assess breakage under different loading conditions, conventional laboratory methods are limited in their ability to capture the internal processes of particle deformation and fracture. Most existing techniques provide only indirect evidence of breakage, such as changes in gradation curves or stress-strain responses, and fail to reveal how particles interact and fracture in real time. These limitations hinder our understanding of the micromechanics driving the observed macro-scale behavior and the development of more accurate constitutive models (Daouadji, Hicher and Rahma, 2001; McDowell and Harireche, 2002; Valdes and Koprulu, 2007; Xu et al., 2022).

In response to these challenges, X-ray computed tomography (XCT) has emerged as a transformative tool for investigating granular materials at the grain scale. XCT enables non-invasive, high-resolution, three-dimensional imaging of soil specimens during loading, offering direct visualization of

internal structural changes, crack formation, and grain rearrangement (Cil and Alshibli, 2012; Alam, Haque and Ranjith, 2018; Karatza et al., 2019). XCT has been successfully used to characterize fracture mechanisms such as splitting, chipping, and full fragmentation, and to examine how these processes are influenced by factors such as particle morphology, coordination number, and mineralogy.

In this study, we utilize XCT in combination with the Deben CT5000, a miniature loading frame designed for use inside a micro-CT scanner, to investigate the deformation and breakage mechanisms of calcareous and glauconitic sands. High-resolution 3D scans were acquired during incremental loading to capture the evolution of microstructural changes in real time. Our objective is to characterize the breakage mechanisms specific to each sand type, compare the particle-scale behavior across different mineralogies, and link these microstructural observations to broader geotechnical responses such as strength development and settlement.

The insights gained from this experimental investigation will improve the mechanistic understanding of particle breakage in crushable sands and support the development of more realistic, microstructure-informed constitutive models. Furthermore, this work has practical implications for the design and analysis of offshore and coastal geotechnical systems, where particle breakage often governs long-term performance and stability (Yasufuku and Hyde, 1995; Xiao et al., 2017; Altuhafi et al., 2018; Mao, Hamaguchi and Koseki, 2020).

2 MATERIALS AND METHODS

This study investigates two classes of crushable sands with distinct mineralogical compositions: glauconitic sands and calcareous sands. The aim was to explore how mineralogical differences influence particle breakage and deformation behavior under compressive loading, as captured by high-resolution X-ray computed tomography (XCT). The following subsections describe the mineralogical characteristics of the tested materials, their grain size distributions, and the experimental setup used to conduct the compression tests and acquire XCT scans.

2.1 *Mineralogy*

The glauconitic sand sample (GL-RS1) was sourced from a natural deposit near Antwerp, Belgium, known for its quartz-dominated sands enriched with glauconite pellets. The glauconite content of GL-RS1 was measured using a Frantz isodynamic magnetic separator at the Department of Geology, Ghent University. The separation was performed with a slope angle of 6°, a tilt angle of 11°, and a current of 0.28 A applied in two passes, enabling the effective concentration of glauconite pellets from the bulk sand matrix. Glauconite is a green, iron-potassium phyllosilicate mineral, typically occurring as rounded, friable pellets. Due to its low hardness and laminated internal structure, glauconite grains are particularly prone to disintegration under stress, which can significantly alter the mechanical response of the surrounding sand matrix.

The calcareous sand samples were collected from the Persian Gulf, a region rich in biogenic carbonate sediments. These sands primarily consist of angular skeletal fragments from marine organisms such as corals and mollusks, with a high calcium carbonate content. Their particles are highly porous and brittle, making them especially susceptible to crushing even under moderate stress levels. The heterogeneity in particle shape and internal porosity further contributes to their complex mechanical behavior.

Representative images of the tested materials, including the calcareous sand (Calc-RAW) and the glauconitic sand (GL-RS1), are shown in Figure 1. These samples differ in texture and coloration, visually reflecting their distinct mineralogical compositions.

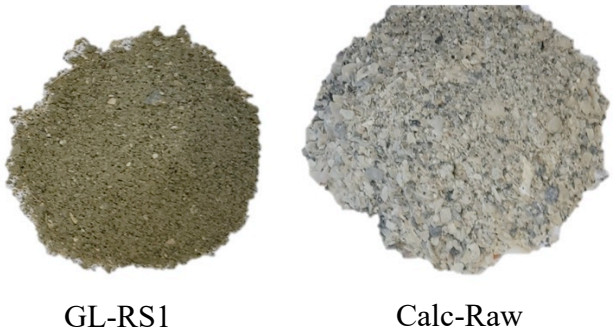

Figure 1. Visual appearance of the tested sand samples: GL-RS1 (14% glauconite), and Calc-Raw (calcareous sand from the Persian Gulf)

2.2 *Grain Size Distribution*

Grain size distribution plays a key role in determining the mechanical behavior of granular soils, especially in the context of particle rearrangement, contact forces, and breakage potential. The grain size distributions of the glauconitic and calcareous sand samples used in this study were determined through wet sieve analysis in accordance with ASTM D6913, and the results are presented in Figure 2.

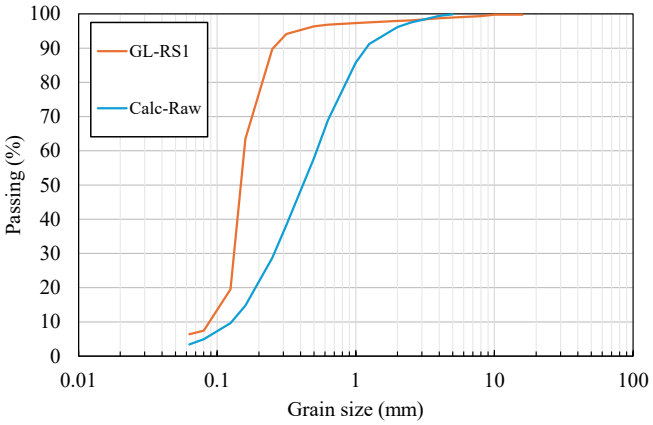

Figure 2. Grain size distribution curves of the tested sands

The glauconitic sand sample (GL-RS1) exhibits a grading curve typical of fine to medium sand, with most particles ranging between 0.1 mm and 0.6 mm. The curve is steep, indicating a relatively narrow particle size range and a tendency toward dense packing. This sample is moderately to well-graded, as evidenced by its steep distribution curves, indicating a narrow particle size range and dense packing potential.

In contrast, the calcareous sand (Calc-Raw) shows a broader and coarser particle size distribution, with grain sizes ranging from below 0.1 mm up to nearly 3 mm. The flatter slope of the curve indicates a poorly graded material with a wider range of particle sizes. This variability arises from the biogenic origin of the sample, composed primarily of fragmented coral, shell, and skeletal materials of varying sizes and shapes. The presence of larger and more porous particles is expected to influence both the initial fabric and the extent of particle breakage during loading.

2.3 *Experimental Setup*

To investigate the micromechanical behavior of crushable sands, compression tests were conducted using the Deben CT5000 micro-mechanical loading stage mounted inside the CoreTom X-ray computed tomography (XCT) scanner at Ghent University's Centre for X-ray Tomography (UGCT). This configuration enabled high-resolution, in-situ 3D imaging of the internal structure of the specimens at key stages of the test.

The Deben CT5000 is a XCT-compatible loading device capable of applying controlled compressive force while allowing high-resolution imaging. In this study, loading was applied under displacement-controlled conditions until a maximum axial force of 2.5 kN was reached. The XCT scans were taken at the start and at the end of the test, providing clear images of the particle arrangement and fracture development before and after compression.

Samples were prepared in transparent polycarbonate cylindrical holders with a 5 cm internal diameter and an initial height of 1.4 cm. To avoid premature particle breakage during sample preparation, special care was taken to achieve the loosest possible packing condition. The sand was gently poured into the container without any tamping or vibration, minimizing interparticle stress and preserving the original grain structure. This step was especially important for both glauconitic and calcareous sands, which are known to be highly crushable.

The dry densities of the specimens were approximately 1.3 g/cm³ for the glauconitic sand and 1.2 g/cm³ for the calcareous sand. These values reflect the intrinsic differences in grain mineralogy and morphology.

The XCT scans were performed using an accelerating voltage of 120 kV, a power of 15 W, and an exposure time of 500 ms per projection. A total of 3501 projections were acquired over a full 360° rotation. The reconstruction of the projections was carried out using Panthera software (XRE TESCAN), resulting in a 3D volume of the samples with a voxel resolution of 10 µm, which allowed clear identification of grain boundaries, contact points, and fracture surfaces. This setup enabled a direct comparison of the initial and final microstructures of the tested materials and provided a basis for evaluating deformation and crushing mechanisms at the particle scale.

Photographs of the experimental setup are shown in Figure 3. The Deben CT5000 loading stage is illustrated in Figure 3a, where the sample holder is positioned for compression inside the CT scanner. Figure 3b shows the CoreTom XCT system, which houses the specimen and the loading stage during the scanning procedure. Together, these systems facilitated the non-destructive analysis of sand behavior under mechanical loading conditions.

3 RESULTS

3.1 *Accuracy of Grain Size Distribution Measurement from XCT Data*

To assess the accuracy of grain size distribution (GSD) measurements obtained from XCT image analysis, the results were compared with those from conventional wet sieve analysis for both the calcareous sand (Calc-Raw) and the glauconitic sand (GL-RS1). The comparisons are shown in Figure 4a for Calc-Raw and Figure 4b for GL-RS1.

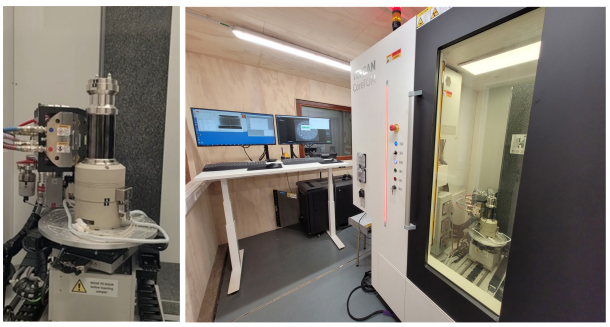

(a) (b)

Figure 3. Experimental setup used for in-situ XCT scanning of crushable sands: (a) Deben CT5000 micro-compression stage mounted for scanning; (b) CoreTom XCT scanner at UGCT, Ghent University.

For the calcareous sand (Figure 4a), the GSD curve obtained from XCT analysis closely matched the sieve analysis results across the entire particle size range, with only minor deviations at the finer fraction (<0.15 mm). The coefficient of determination (R^2) between the two methods was 0.991, indicating excellent agreement.

For the glauconitic sand (GL-RS1), the XCT-derived GSD also exhibited strong consistency with the sieve-derived distribution. Slight differences were observed in the fine fraction (<0.1 mm), which may be attributed to resolution limitations of the CT imaging and segmentation thresholds. The overall correlation between the two methods was very high, with an R^2 value of 0.986.

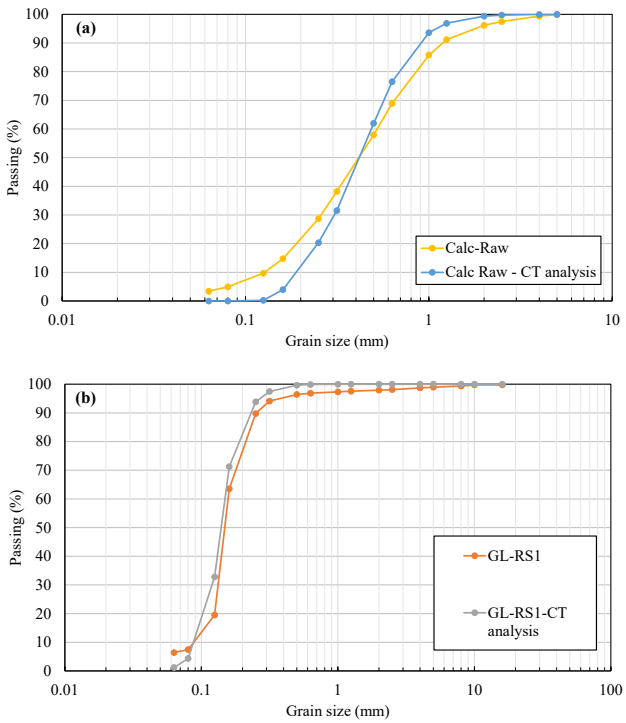

Figure 4. Comparison of grain size distribution (GSD) curves obtained from XCT analysis and sieve analysis: (a) calcareous sand (Calc-Raw), (b) glauconitic sand (GL-RS1).

These results confirm that XCT-based particle size measurement can reliably reproduce the grain size distribution obtained from standard sieving procedures for both calcareous and glauconitic sands. In our case, the average grain diameters

(D_{50}[1]) were approximately 0.149 mm for the glauconitic sand and 0.425 mm for the calcareous sand, corresponding to about 15 and 43 voxels respectively at the 10 µm resolution used in this study— above the minimum of ~12 voxels over the particle sieve size recommended by Burgmann et al. (2021), to maintain <5% expanded measurement uncertainty for particle length at 90% confidence. Moreover, unlike sieving, XCT can capture the true 3D size and shape of grains, which can reduce the potential bias for elongated or irregular particles that might pass through smaller sieve despite having larger equivalent diameters. This provides confidence in the use of XCT data for subsequent breakage analysis and particle-scale investigations in this study.

3.2 *Effect of Crushing on Grain Size Distribution*

The influence of particle breakage on grain size distribution (GSD) was evaluated by comparing the XCT-derived GSD of the initial specimens with that obtained after the compression tests for both calcareous and glauconitic sands. The results are shown in Figure 5a for the calcareous sand (Calc-Raw) and Figure 5b for the glauconitic sand (GL-RS1).

For the calcareous sand, significant changes in GSD were observed after loading. The post-crushing curve shifted noticeably toward the finer particle sizes, indicating substantial generation of fines and fragmentation of coarser grains. This shift was particularly pronounced for particles in the size range of 0.2–1.0 mm, suggesting that medium-sized skeletal fragments were highly susceptible to crushing under the applied load. The increase in the proportion of fines (<0.1 mm) reflects the brittle nature and high porosity of calcareous grains, which readily fractured into smaller particles.

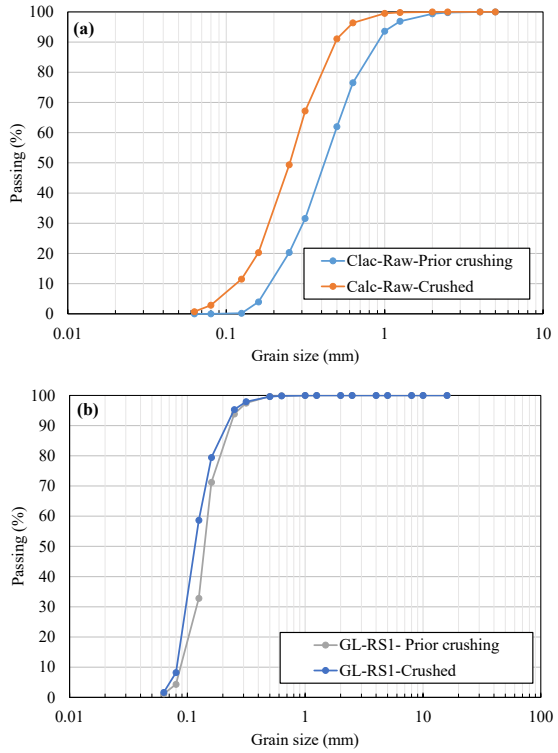

Figure 5. Effect of crushing on grain size distribution for (a) calcareous sand (Calc-Raw) and (b) glauconitic sand (GL-RS1).

In contrast, the glauconitic sand (GL-RS1) showed minimal changes in GSD after loading. The post-crushing curve almost overlapped the initial distribution, with only a slight increase in fines below 0.1 mm. This limited breakage suggests that, under the applied loading conditions, the coarse fraction remained largely intact. The smaller degree of change compared to the calcareous sand could be attributed to the more compact quartz-glauconite framework, where quartz grains provide resistance to further crushing once initial rearrangements occur.

3.3 *Effect of Sample Type on Particle Breakage Index*

The extent of particle breakage for each sand type was quantified using Hardin's Relative Breakage Index (Br) (Hardin, 1985). This method evaluates the proportion of the total breakage (B_t) to the breakage potential (B_p) based on changes in grain size distribution (GSD) before and after loading.

- Breakage potential (B_p) is the area between the initial GSD curve and a reference line representing the maximum possible breakage, typically taken as a vertical line at the smallest particle size considered (here 0.074 mm).
- Total breakage (B_t) is the area between the initial and final GSD curves.
- The relative breakage is calculated in eq.1:

$$B_r = \frac{B_t}{B_p} \quad \text{(eq.1)}$$

A schematic of Hardin's method is shown in **Figure 6**, where B_t is represented by the hatched area between the initial and current grading curves, and Bp is the shaded area representing the maximum potential breakage.

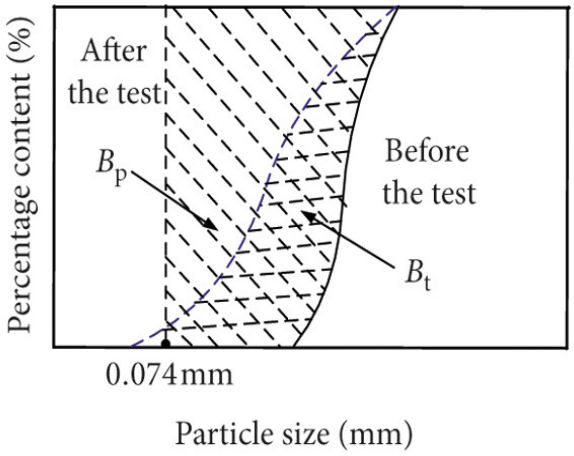

Figure 6. Schematic of Hardin's method for calculating the particle breakage index (Br) from initial and final grain size distribution curves (Xu et al., 2022).

Applying this method to the tested materials, the calcareous sand exhibited a Br value of 0.280, while the glauconitic sand (GL-RS1) had a lower value of 0.171. These results confirm that the calcareous sand is significantly more crushable under the applied loading conditions. The higher breakage in the calcareous sand can be attributed to its biogenic carbonate composition, high porosity, and brittle skeletal fragments,

[1] D_{50} refers to the particle size at which 50% of the sample by weight is finer, as determined from the cumulative grain size distribution curve

which readily fracture under stress. In contrast, the glauconitic sand's lower Br value reflects a more resistant mineral framework dominated by quartz grains, which limits extensive crushing despite the presence of weaker glauconite pellets.

This difference in breakage behavior is consistent with the GSD shifts observed in Section 3.2 and highlights the need to consider mineralogical composition when evaluating crushable sands in geotechnical applications.

4 CONCLUSION

This study employed high-resolution X-ray computed tomography (XCT) combined with in-situ compression testing to investigate the deformation and breakage behavior of two crushable sands with distinct mineralogies: calcareous sand from the Persian Gulf and glauconitic sand (GL-RS1) from Antwerp, Belgium.

Validation of XCT-based grain size distribution (GSD) analysis against conventional wet sieve measurements demonstrated excellent agreement, with R^2 values of 0.991 for calcareous sand and 0.986 for glauconitic sand. This confirms that, for our setup, sample properties, and the obtained spatial resolution, XCT can accurately quantify particle size characteristics. However, this accuracy depends on factors such as sample diameter, grain size distribution, XCT acquisition parameters, and the resulting spatial resolution.

Under compressive loading to 2.5 kN, the calcareous sand exhibited substantial particle breakage, reflected by a marked shift in its GSD toward finer fractions and a high relative breakage index (Br=0.280). The glauconitic sand displayed only minimal changes in GSD, with a significantly lower breakage index (Br=0.171). These differences are attributed to the calcareous sand's biogenic carbonate composition, high porosity, and brittle skeletal fragments, which readily fractured under stress, versus the more resistant quartz–glauconite framework of the glauconitic sand.

The results highlight that mineralogical composition exerts a primary control on crushability and associated changes in particle size distribution. For geotechnical applications, particularly in offshore foundations where long-term stability is critical, materials with higher breakage susceptibility, such as calcareous sands, require careful consideration in design to account for potential changes in packing density, permeability, and strength.

Future work will extend this analysis to additional glauconitic samples and incorporate 4D XCT imaging to capture the full temporal evolution of particle breakage mechanisms during loading.

5 ACKNOWLEDGEMENTS:

The authors acknowledge the Centre for X-ray Tomography (BOF.COR.2022.0008) and IOF (project FaCT, F2021/IOF-Equip/021) for providing access to XCT data acquisition facilities. The Research Foundation – Flanders (FWO, project G.0041.15N) and the Faculty of Sciences, FCWO – Ghent University, are acknowledged for the Deben CT5000 in-situ loading device. This project has received funding from the European Union's Horizon Europe research and innovation programme under grant agreement No 101131765 (EXCITE2) for Transnational Access conducted at the Centre for X-ray Tomography (UGCT), Ghent University.

6 REFERENCES

Alam, M.F., Haque, A. and Ranjith, P.G., 2018. A study of the particle-level fabric and morphology of granular soils under one-dimensional compression using insitu X-ray CT imaging. *Materials*, 11(6), p.919.

Altuhafi, F.N., Jardine, R.J., Georgiannou, V.N. and Moinet, W.W., 2018. Effects of particle breakage and stress reversal on the behaviour of sand around displacement piles. *Géotechnique*, 68(6), pp.546–555. https://doi.org/10.1680/jgeot.17.P.117.

Belousov, P.E., Chupalenkov, N.M., Rudmin, M.A. and Krupskaya, V.V., 2022. Glauconite Deposits in Russia: Geological Position, Formation Conditions, and Development Perspectives. *Lithology and Mineral Resources*, 57(3), pp.234–247. https://doi.org/10.1134/S002449022202002X.

Burgmann, S., Godehardt, M., Schladitz, K. and Breit, W., 2021. Influence of voxel size for µCT imaging of particles on measurement accuracy. *Construction and Building Materials*, 289, p.123148. https://doi.org/10.1016/j.conbuildmat.2021.123148.

Cil, M.B. and Alshibli, K.A., 2012. 3D assessment of fracture of sand particles using discrete element method. *Géotechnique Letters*, 2(3), pp.161–166. https://doi.org/10.1680/geolett.12.00024.

Coop, M. and Atkinson, J., 1993. The mechanics of cemented carbonate sands. *Geotechnique*, 43(1), pp.53–67.

Coop, M.R., Sorensen, K.K., Bodas Freitas, T. and Georgoutsos, G., 2004. Particle breakage during shearing of a carbonate sand. *Géotechnique*, 54(3), pp.157–163. https://doi.org/10.1680/geot.2004.54.3.157.

Daouadji, A., Hicher, P.-Y. and Rahma, A., 2001. An elastoplastic model for granular materials taking into account grain breakage. *European Journal of Mechanics-A/Solids*, 20(1), pp.113–137.

Folk, R.L., 1980. *Petrology of sedimentary rocks*. Hemphill publishing company.

Hagerty, M., Hite, D., Ullrich, C. and Hagerty, D., 1993. One-dimensional high-pressure compression of granular media. *Journal of Geotechnical Engineering*, 119(1), pp.1–18.

Hardin, B.O., 1985. Crushing of Soil Particles. *Journal of Geotechnical Engineering*, 111(10), pp.1177–1192. https://doi.org/10.1061/(ASCE)0733-9410(1985)111:10(1177).

Heiken, G., 1974. Atlas of volcanic ash. *Smithsonian Contributions to the Earth Sciences*.

Indraratna, B., Wijewardena, L. and Balasubramaniam, A., 1993. Large-scale triaxial testing of grey wacke rockfill. *Geotechnique*, 43(1), pp.37–51.

Jia, Y., Xu, B., Chi, S., Xiang, B., Xiao, D. and Zhou, Y., 2019. Particle Breakage of Rockfill Material during Triaxial Tests under Complex Stress Paths. *International Journal of Geomechanics*, 19(12), p.04019124. https://doi.org/10.1061/(ASCE)GM.1943-5622.0001517.

JM, D.S., 1958. Compressibility of sand at high pressure. *MS thesis, Massachusetts Institute of Technology*, pp.63–64.

Karatza, Z., Andò, E., Papanicolopulos, S.-A., Viggiani, G. and Ooi, J.Y., 2019. Effect of particle morphology and contacts on particle breakage in a granular assembly studied using X-ray tomography. *Granular Matter*, 21(3), p.44. https://doi.org/10.1007/s10035-019-0898-2.

Le Pera, E. and Morrone, C., 2020. The use of mineral interfaces in sand-sized volcanic rock fragments to infer mechanical durability. *Journal of Palaeogeography*, 9(1), p.21. https://doi.org/10.1186/s42501-020-00068-8.

Lee, K.L. and Farhoomand, I., 1967. Compressibility and crushing of granular soil in anisotropic triaxial compression. *Canadian geotechnical journal*, 4(1), pp.68–86.

Mao, W., Hamaguchi, H. and Koseki, J., 2020. Discrimination of Particle Breakage below Pile Tip after Model Pile Penetration in Sand Using Image Analysis. *International Journal of Geomechanics*, 20(1), p.04019142. https://doi.org/10.1061/(ASCE)GM.1943-5622.0001535.

Marsal, R.J., 1967. Large Scale Testing of Rockfill Materials. *Journal of the Soil Mechanics and Foundations Division*, 93(2), pp.27–43. https://doi.org/10.1061/JSFEAQ.0000958.

McDowell, G., Bolton, M. and Robertson, D., 1996. The fractal crushing of granular materials. *Journal of the Mechanics and Physics of Solids*, 44(12), pp.2079–2101.

McDowell, G. and Harireche, O., 2002. Discrete element modelling of soil particle fracture. *Géotechnique*, 52(2), pp.131–135.

Nakata, Y., Hyodo, M., Hyde, A.F.L., Kato, Y. and Murata, H., 2001. Microscopic Particle Crushing of Sand Subjected to High Pressure

One-Dimensional Compression. *Soils and Foundations*, 41(1), pp.69–82. https://doi.org/10.3208/sandf.41.69.

Peng, Y., Yin, Z.-Y., Yang, F., Qu, L. and Ding, X., 2024. Analysis of the effect of breakable particle corners on uplift pile–soil interaction behaviors in calcareous sand. *Acta Geotechnica*, 19(11), pp.7307–7328. https://doi.org/10.1007/s11440-024-02367-z.

Scoffin, T.P., 1987. Introduction to carbonate sediments and rocks.

Seed, H.B. and Lee, K.L., 1967. Undrained strength characteristics of cohesionless soils. *Journal of the Soil Mechanics and Foundations Division*, 93(6), pp.333–360.

Terzaghi, K. and Peck, R.B., 1948. Soil mechanics. *Engineering Practice. John Wiley and Sons, Inc., New York*.

Valdes, J.R. and Koprulu, E., 2007. Characterization of fines produced by sand crushing. *Journal of geotechnical and geoenvironmental engineering*, 133(12), pp.1626–1630.

Vesić, A.S. and Clough, G.W., 1968. Behavior of granular materials under high stresses. *Journal of the Soil Mechanics and Foundations Division*, 94(3), pp.661–688.

Wu, Y., Li, N., Wang, X., Cui, J., Chen, Y., Wu, Y. and Yamamoto, H., 2021. Experimental investigation on mechanical behavior and particle crushing of calcareous sand retrieved from South China Sea. *Engineering Geology*, 280, p.105932. https://doi.org/10.1016/j.enggeo.2020.105932.

Xiao, Y., Liu, H., Chen, Q., Ma, Q., Xiang, Y. and Zheng, Y., 2017. Particle breakage and deformation of carbonate sands with wide range of densities during compression loading process. *Acta Geotechnica*, 12(5), pp.1177–1184. https://doi.org/10.1007/s11440-017-0580-y.

Xu, L.-J., Wang, R., Xu, D.-S., Wang, X.-Z., Meng, Q.-S. and Zhu, C.-Q., 2022. Review of Particle Breakage Measurement Methods for Calcareous Sand. *Advances in Civil Engineering*, 2022(1), p.6477197. https://doi.org/10.1155/2022/6477197.

Yasufuku, N. and Hyde, A.F.L., 1995. Pile end-bearing capacity in crushable sands. *Géotechnique*, 45(4), pp.663–676. https://doi.org/10.1680/geot.1995.45.4.663.

Zimbelman, D.R., 1996. *Hydrothermal alteration and its influence on volcanic hazards--Mount Rainier, Washington, a case history*. University of Colorado at Boulder.